npj | climate and atmospheric science

www.nature.com/npjclimatsci

ARTICLE OPEN

Check for updates

Geostationary satellite reveals increasing marine isoprene emissions in the center of the equatorial Pacific Ocean

Wentai Zhang [1] and Dasa Gu [1,2]✉

Isoprene is the most abundant non-methane biogenic volatile organic compound in the Earth's atmosphere and has the potential to influence photochemistry in the remote ocean–atmosphere. Marine isoprene emission estimates vary over multiple orders of magnitude using different methods, and the paucity of continuous in-situ measurements makes it challenging to distinguish their spatiotemporal variations. Here we present marine isoprene emission estimates inferred from Himawari-8 observations and model simulation covering the western Pacific Ocean and the eastern Indian Ocean. Although most isoprene emission hotspots were near coasts, we found an unexpected emission pool in the center of the equatorial Pacific Ocean with 18% higher emissions than those in the North and South Pacific Oceans. Remarkably, the isoprene emissions increased by 5.5 ± 0.1% per year in the center of the equatorial Pacific Ocean between August 2015 and December 2020, while no significant trend for emissions in other ocean regions. We investigated marine isoprene oxidation impacts based on satellite observations, and the results suggest NO_2 may play a critical role during aerosol formation from isoprene in the remote ocean air.

npj Climate and Atmospheric Science (2022)5:83 ; https://doi.org/10.1038/s41612-022-00311-0

INTRODUCTION

Isoprene (2-methyl-1,3-butadiene, C_5H_8) is an active volatile organic compound (VOC) that has significant impacts on global climate, either through cloud formation[1–3] or cloud inhibition[4,5]. While terrestrial vegetation is the primary emission source of atmospheric isoprene[6,7], marine-originated isoprene potentially influences secondary organic aerosol (SOA) formation in the remote ocean, especially in association with increased emissions during phytoplankton blooms[1,8–10]. SOA produced by photooxidation of marine isoprene affects the coastal regions most and can reach as far as hundreds of kilometers inland[11], altering the air quality of impacted regions[12].

Marine isoprene has a strong biogenic origin[13,14]. Phytoplankton are suggested to be the chief marine isoprene emission source, though heterotrophic bacteria and seaweeds can also emit isoprene[15]. The dependence of phytoplankton isoprene production on phytoplankton biomass[9,16], phytoplankton functional types (PFTs)[17,18], and environmental drivers (e.g., light and temperature)[19–21] have been investigated in laboratory incubation experiments[19,22], mesocosm studies[23], and in-situ measurements[16,24,25].

To better quantify the impacts of marine isoprene on atmospheric chemistry and global climate, marine isoprene emission needs to be better constrained. While bottom-up[22,26–28] and top-down[26,29] methods have been applied to estimate marine isoprene emissions, there are still significant discrepancies (two orders of magnitude) among previous estimates due to the paucity of continuous in-situ measurements and limited understanding of mechanisms involved in marine isoprene production and loss[26,30]. Although some field measurements[31,32] and lab experiments[33] proposed that photochemical reactions occurring in the sea surface microlayer (SML) may account for the discrepancies[34], underway eddy covariance measurements of marine isoprene emission fluxes in the Northern Atlantic Ocean do not show a statistically significant correlation with shortwave radiation[35].

Here, we report marine isoprene emission fluxes estimated from satellite observations and model simulation over a study region covering the western Pacific Ocean and the eastern Indian Ocean (120°E–160°W, 60°S–60°N, Supplementary Fig. 1a) from August 2015 to December 2020. The marine isoprene emission model was established based on a PFT-specific isoprene production module which incorporates both light and temperature dependency (Fig. 1). The 3-D temperature structure in the euphotic zone was reconstructed from remotely sensed sea surface temperature (SST), sea surface height (SSH), and wind stress (WS) measurements. Afterward, dynamic mixed layer depth was derived from the 3-D temperature structure by using the temperature threshold method[36]. As the light and temperature vary with water depth, the isoprene production in the mixed layer was quantified by integrating the isoprene produced at all water column depths within the mixed layer. Isoprene flux from SML was calculated by estimating the photochemical isoprene production occurring in the SML. The satellite observation data from Himawari-8 L3 (i.e., chlorophyll-a (Chl-a) concentrations, SST, photosynthetically active radiation (PAR)) were used for model simulation. Utilizing high-resolution geostationary satellite observations, this work proposes to: (1) elucidate the spatial and temporal distributions of marine isoprene over the western Pacific Ocean and the eastern Indian Ocean; (2) quantify the trends of marine isoprene emissions and investigate contributions from biological and physical environment parameters; (3) assess the potential impacts from marine isoprene emissions on air quality and climate. We observed significantly high marine isoprene emission flux (7.4 nmol m^{-2} h^{-1}) in the center of the equatorial Pacific Ocean (CEPO, $7°S \sim 5°N$, $175°E \sim 160°W$, Supplementary Fig. 1). At the same time, the trend of isoprene emission was also remarkably high (5.5 ± 0.1% yr^{-1}) during 65 months period in the same region. The results reveal significant positive correlations between

[1]Division of Environment and Sustainability, The Hong Kong University of Science and Technology, Hong Kong, China. [2]Guangdong-Hongkong-Macau Joint Laboratory of Collaborative Innovation for Environmental Quality, The Hong Kong University of Science and Technology, Hong Kong, China. ✉email: dasagu@ust.hk

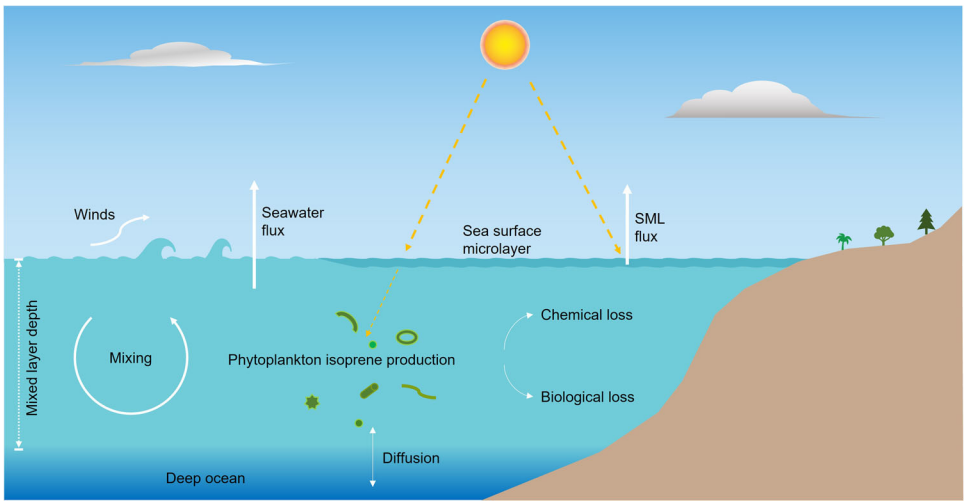

Fig. 1 Schematic diagram of marine isoprene emission model in the upper ocean. The model includes modules of phytoplankton isoprene production, chemical loss, biological loss, diffusion to the deeper ocean, seawater isoprene flux, and SML isoprene flux.

isoprene emission flux and some environmental parameters (wind speed, Chl-a concentration, and PAR) in CEPO, while negative correlations between isoprene emission flux and SST. The contribution of marine isoprene emission on aerosol was also investigated, indicating their essential roles in changing the atmospheric oxidation process in the remote ocean.

RESULTS

Marine isoprene emission flux

We calculated the mean values of marine isoprene emission flux, seawater flux, and SML flux for each grid cell over the 65 months between August 2015 and December 2020, as shown in Fig. 2a–c. Comparing different ocean regions (Supplementary Fig. 1a), the marine isoprene emission flux shown in Fig. 2a and seawater isoprene flux shown in Fig. 2b exhibit similar spatial patterns. The mean values of marine isoprene emission flux in coastal regions (6.5 nmol m^{-2} h^{-1}) were at approximately the same level as that in open ocean regions (6.4 nmol m^{-2} h^{-1}). Comparing between major open ocean areas, the marine isoprene emission flux in the East Indian Ocean (EIO) was higher than that in the North Pacific Ocean (NPC) and the South Pacific Ocean (SPC), which were 6.9, 6.2, and 6.2 nmol m^{-2} h^{-1}, respectively (Supplementary Table 3). The contributions from seawater isoprene flux to marine isoprene flux were between 70% and 85% in most ocean areas and can reach as high as 90% in some coastal regions (Supplementary Fig. 2). The mean value of marine isoprene emission flux in the ocean areas is 6.5 nmol m^{-2} h^{-1}, which was extrapolated for a global estimate (1.2 Tg C yr^{-1}) by multiplying the area ratio in spite of the large uncertainties involved. The comparisons of our estimates with the results reported in previous studies are provided in Supplementary Table 2.

Remarkably, there were significantly higher marine isoprene emission flux in CEPO and the Tasman Sea, which were 7.4 and 8.7 nmol m^{-2} h^{-1} (Supplementary Table 3). While the marine isoprene flux in CEPO and Tasman sea were about 20% and 40% higher than that in NPC and SPC, the seawater isoprene concentrations in the Tasman Sea (62.7 pmol L^{-1}) were about 26% lower than that in CEPO (84.2 pmol L^{-1}). It suggests the air–sea transfer rate has higher sensitivity of wind speed than SST (see SI Eqs. (2) and (3)), as the wind speeds in CEPO and the Tasman Sea were around 5.6 and 8.3 m s^{-1}, respectively (Supplementary Fig. 2), and SST in two regions were ~28.7 and 16.3 °C (Fig. 2e).

Figure 2c shows that the SML fluxes in subtropical areas of NPC, EIO, and coastal regions of Australia were higher than 1.8 nmol m^{-2} h^{-1}. In comparison, SML fluxes in the NPC's equatorial and high-latitude region were merely around 1.2 nmol m^{-2} h^{-1}. The Chl-a concentrations were lower than 0.1 mg m^{-3} in most open oceans (Fig. 2d), but the values could reach 0.3 mg m^{-3} in CEPO and the high-latitude Pacific Ocean. In coastal regions, the Chl-a concentrations can be higher than 0.4 mg m^{-3}, generally due to larger nutrient supplies. In Fig. 2e, the sea surface temperature (SST) was highest (≥30 °C) in the equatorial region and decreased to the lowest value (about 0 °C) with increasing latitude. In Fig. 2f, the photosynthetically available radiation (PAR) value in the equatorial and subtropical ocean (>400 μmol m^{-2} s^{-1}) was higher than in high-latitude regions. The mean values of the associated parameters in CEPO can be found in Supplementary Table 5. Climatological marine isoprene emissions, seawater isoprene emissions, and SML emissions are displayed in Supplementary Figs. 8, 9, and 10, respectively.

Increasing emission trends over the equatorial Pacific Ocean

The trend significance of the time series was detected at each grid cell using the Mann–Kendall (MK) test[37]. The magnitude of the linear trend was estimated by the Theil–Sen estimator[38,39]. While the marine isoprene emission flux in most open ocean areas showed insignificant trends, remarkable increasing trends were discovered in CEPO (Fig. 3). The mean values of absolute and relative marine isoprene emission flux trends were 401 ± 4 pmol m^{-2} h^{-1} yr^{-1} and 5.5 ± 0.1% yr^{-1} in CEPO (Fig. 3a, d). The mean values of seawater isoprene flux's absolute and relative trends in CEPO were 342 ± 4 pmol m^{-2} h^{-1} yr^{-1} and 5.9 ± 0.1% yr^{-1} (Fig. 3b, e). The spatial patterns of seawater isoprene flux trends were very similar to marine isoprene emission flux (Fig. 3a, b, d, e), highlighting its main contribution to marine isoprene emission flux. Although the trends of SML flux in most ocean areas were insignificant, there were notably increasing trends of SML flux in CEPO (Fig. 3c, f). The mean values of the absolute and relative trend of SML flux in CEPO were 75 ± 1 pmol m^{-2} h^{-1} yr^{-1} and 5.0 ± 0.1% yr^{-1}. The complete list of the trends in marine isoprene emissions of the selected open oceans is given in Supplementary Table 4.

To explore the driving factors of notable increasing trends of isoprene flux in CEPO, we investigated the temporal and spatial variations of biological and physical environment parameters (Fig. 4a–d). The Chl-a concentrations in most open ocean areas were decreasing except for CEPO, where the mean value of the relative

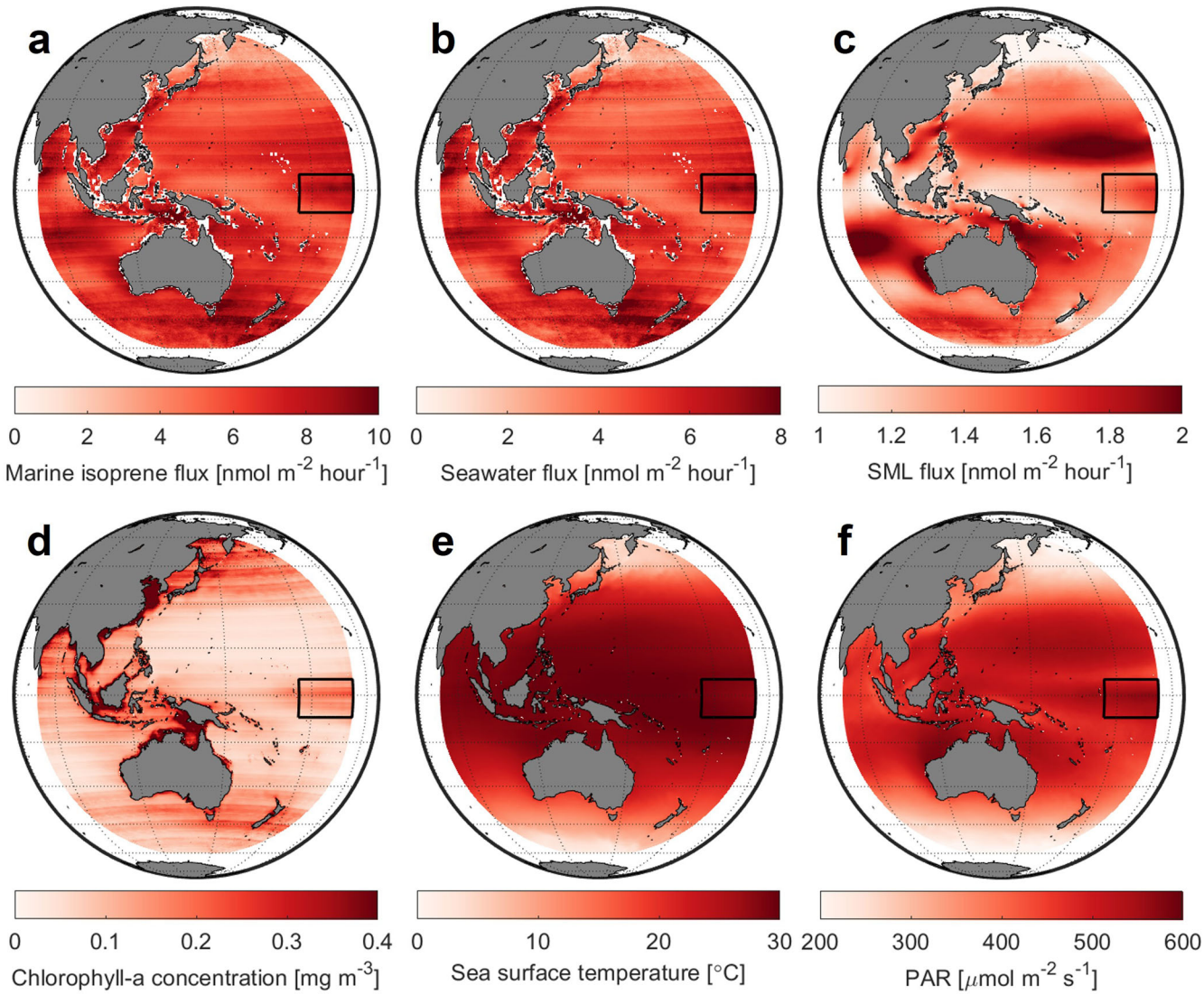

Fig. 2 Mean values of isoprene emission fluxes and major environmental drivers from August 2015 to December 2020. a Marine isoprene emission flux. **b** Seawater flux. **c** SML flux. **d** Chl-a concentrations. **e** Sea surface temperature. **f** PAR.

trends was $7.1 \pm 0.1\%\ yr^{-1}$ (Fig. 4a). The mean value of SST relative trends in CEPO was $-8.8 \pm 0.1‰\ yr^{-1}$, while in most ocean regions, the relative trends were insignificant (Fig. 4b). The PAR in CEPO had remarkable positive trends, and the mean value was $20.1 \pm 0.2‰\ yr^{-1}$ (Fig. 4c). In Fig. 4d, the relative wind speed trend was significant in CEPO, and the mean value was $44.4 \pm 0.4‰\ yr^{-1}$. The patterns above suggest prominent impacts from four major environmental parameters on the notable increase in isoprene emission trends in CEPO. The entire list of the absolute and relative trends in environmental parameters in CEPO can be found in Supplementary Tables 6 and 7.

The correlations between marine isoprene emission flux and the primary environmental drivers (i.e., Chl-a concentration, SST, PAR, and wind speed) were calculated for detailed investigation (Fig. 4e–h). Unsurprisingly, the marine isoprene emissions were positively correlated with Chl-a concentrations in most open oceans (see Fig. 4e) because Chl-a concentration is a proxy of phytoplankton biomass for primary productivity. Conversely, the negative correlations between marine isoprene emission flux and Chl-a concentrations were found in some coastal areas, suggesting there could be substantial isoprene consumption in the surface of the coastal regions, which is consistent with previous findings[40]. While most tropical and subtropical ocean areas had negative correlations between marine isoprene flux and SST, positive correlations were found in high-latitude ocean areas (Fig. 4f). The isoprene production rate of phytoplankton has been found to increase with temperature until optimum temperature and fall thereafter[19,21]. Ocean areas that show positive correlation might be because the seawater temperature is lower than the optimum temperature for production, while negative correlation might be due to that the seawater temperature is higher than the optimum temperature. In Fig. 4g, marine isoprene emission flux had strong positive correlations with PAR in CEPO and Tasman Sea. Although both seawater isoprene flux and SML flux had a positive relationship with PAR (Eq. (1) and SI Eqs. (4) and (5)), there were negative correlations between marine isoprene emission flux and PAR in the Bay of Bengal, South China Sea, and the Philippine Sea. The variable thermal traits among phytoplankton species and adaptive migrations could alter community composition[41–43], resulting in the biomass change and shift of dominant PFT. One explanation for the negative correlation is that the migrated PFT with a high isoprene emission factor favors low light intensity conditions or high light intensity cooccurs with lower biomass in some ocean areas. As high-speed wind ($\geq 13\ m\ s^{-1}$) tends to disturb the SML formation by breaking waves[34], the negative correlation between marine isoprene emission flux and PAR also

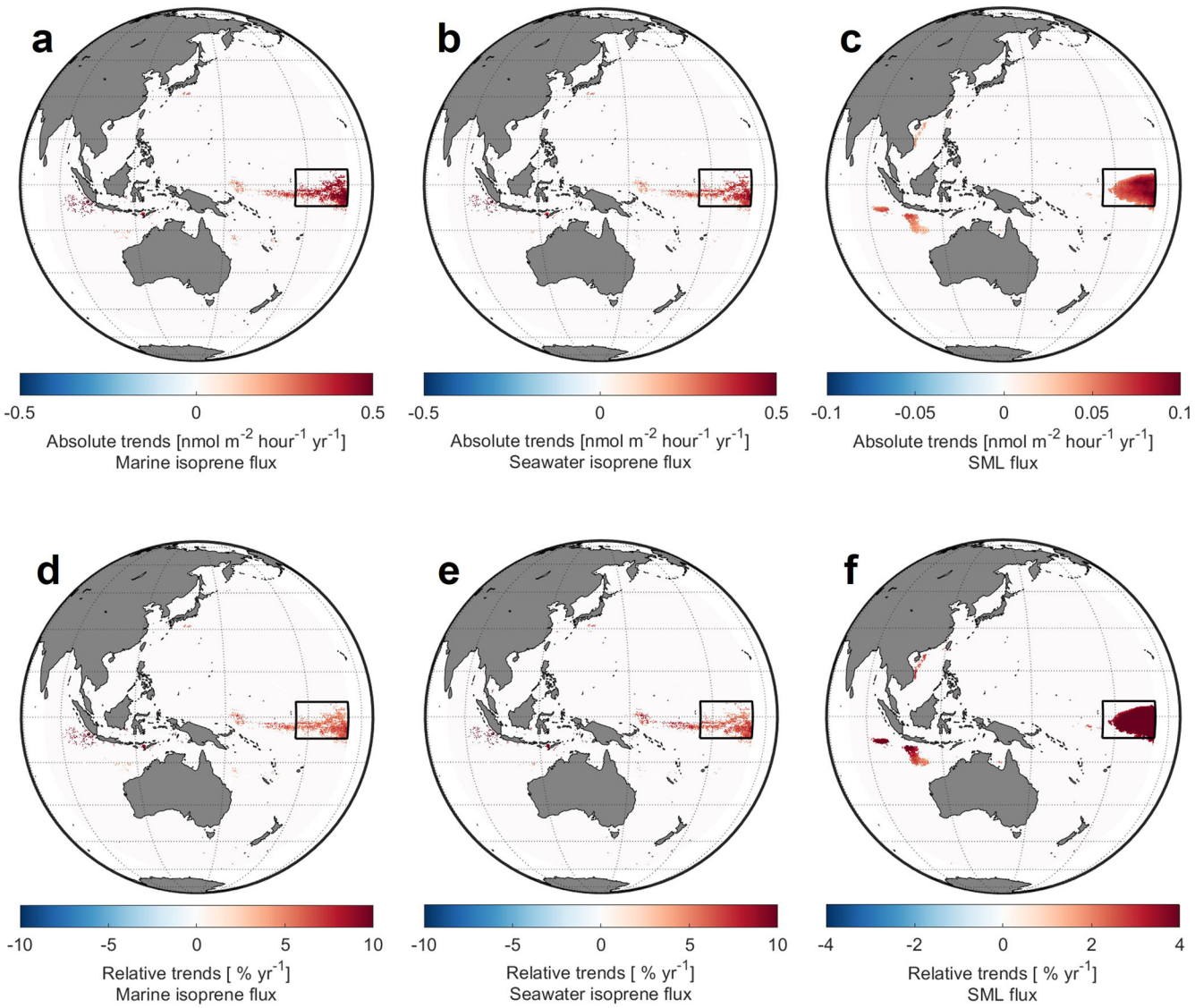

Fig. 3 Absolute and relative trends of isoprene emission fluxes from August 2015 to December 2020. a Absolute trends of marine isoprene emission flux. **b** Absolute trends of seawater isoprene flux. **c** Absolute trends of SML flux. **d** Relative trends of marine isoprene emission flux. **e** Relative trends of seawater isoprene flux. **f** Relative trends of SML flux.

could result from the coincidence of high-speed wind and high PAR, leading to the disruption of SML and negligible SML flux. Figure 4h shows that the correlation coefficients between marine isoprene emission flux and wind speed were positive in latitudes lower than 30° and negative in latitudes higher than 30°. Sea surface wind enhances air–sea gas exchange, and the gas exchange rate becomes more considerable. As wind can also drive the vertical mixing of the ocean, deepening the mixed layer, the seawater isoprene concentration C_w thus tends to be lower. The two mechanisms result in the increase or decrease of the seawater isoprene flux. The complete list of correlation coefficients between marine isoprene emission flux and main parameters in CEPO is shown in Supplementary Table 8.

Impacts on regional atmospheric chemistry and climate

Marine aerosols alter the Earth's climate directly by scattering and absorbing solar radiation and indirectly by changing the formation and properties of clouds over the oceans[44]. Primary sea spray aerosols (SSA) and secondary marine aerosols (SMA) are two major types of marine aerosols. The analysis of aerosol number size distributions from global scale cruise measurements revealed that SSA makes a small contribution to cloud condensation nuclei (CCN) population, especially in tropical regions (around 5.0%)[45]. Mesocosm experiments also suggested that SMA plays the dominant role over SSA in affecting the cloud properties in marine environment[46]. Based on the variability analysis of chemical constituents and their ratios during the phytoplankton bloom of the mesocosm experiments, a hypothesis was further made that SMA could be easily affected by the oxidation of non-DMS VOCs such as isoprene[46].

The isoprene oxidation chain involves complex reactions and varies considerably with local atmospheric conditions[47]. Significant positive correlations have been observed between isoprene fluxes at the cruise track and satellite aerosol optical depth (AOD) of the forward trajectories in the western tropical Indian Ocean during the summer monsoon[48]. To explore isoprene oxidation mechanisms under pristine conditions, we investigated the distribution of OMI tropospheric NO_2 and O_3[49] column densities as functions of Himawari-8 AOD (at 500 nm) and the estimated marine isoprene emission flux in CEPO (Fig. 5). Marine isoprene emission flux had general positive correlations with AOD in most

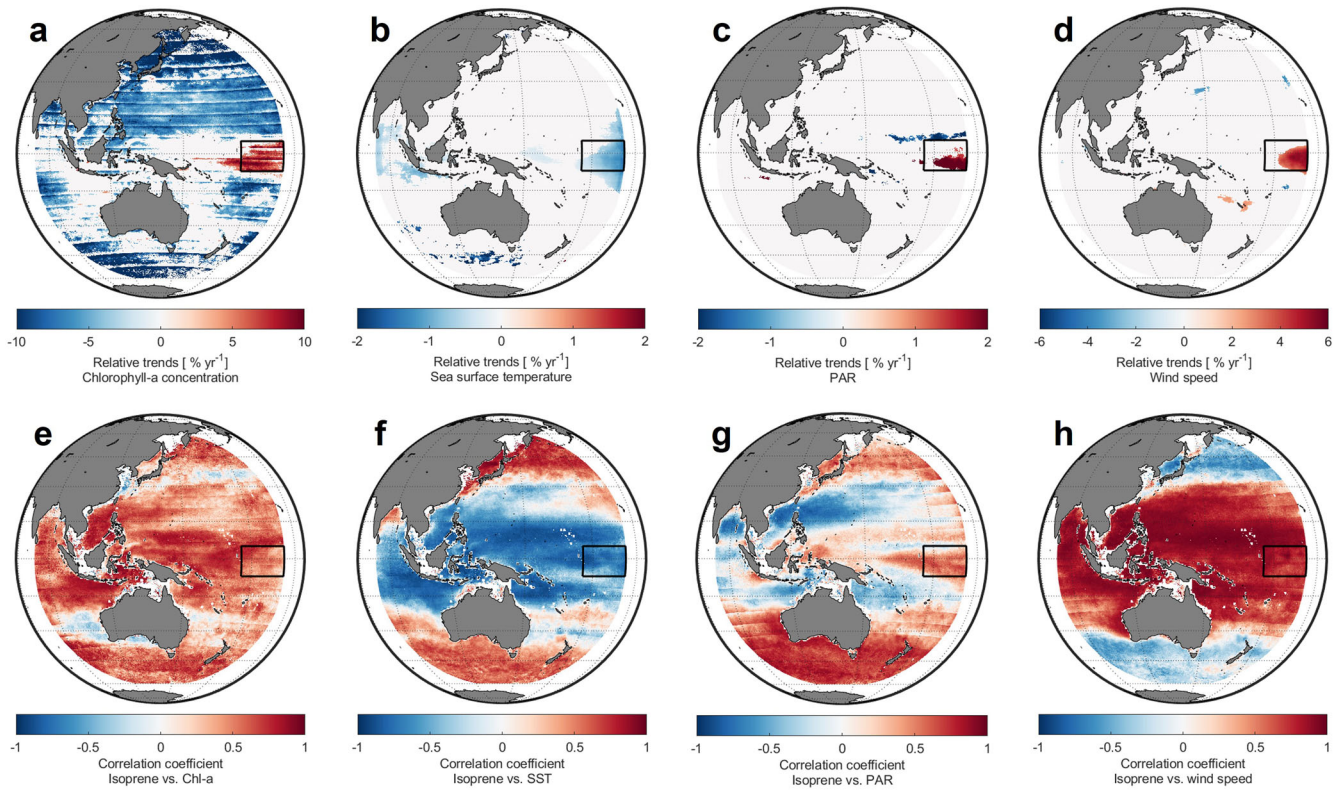

Fig. 4 Relative trends of environmental parameters and their correlation with marine isoprene emission flux from August 2015 to December 2020. a Relative trends of Chl-a concentration. **b** Relative trends of SST. **c** Relative trends of PAR. **d** Relative trends of wind speed. **e** Correlation coefficients between marine isoprene emission flux and Chl-a concentration. **f** Correlation coefficients between marine isoprene emission flux and SST. **g** Correlation coefficients between marine isoprene emission flux and PAR. **h** Correlation coefficients between marine isoprene emission flux and wind speed.

of the ocean areas (Supplementary Fig. 4a), while previous studies found isoprene epoxydiols (IEPOX) can be an intermediate of isoprene-derived SOA formation under low nitrogen oxides ($NO_x = NO + NO_2$) conditions[50].

As shown in Fig. 5a, NO_2 plays a critical role in controlling the SOA yields from isoprene oxidation in CEPO. When NO_2 column densities were higher than 2.5×10^{14} molecules cm^{-2}, rapid enhancements (dashed regression line. slope: 1.5E-2, R-squared: 0.42, *P* value: 0) of AOD were observed with moderate isoprene emissions. As NO_2 column densities dropped below 2.4×10^{14} molecules cm^{-2}, significantly increasing marine isoprene emissions could only lead to much weaker enhancements (solid regression line. slope: 4.4E-3, R-squared: 0.065, *P* value: 0) of AOD. It suggests NO_2 may act as a catalyst during aerosol formation from isoprene in the remote ocean air. Tropospheric ozone column densities were lower than the average level (about 34.5 DU) when both high marine isoprene emission flux (>8.0 nmol m^{-2} h^{-1}) and AOD (≥0.15) were observed in CEPO (Fig. 5b). This suggests that the higher isoprene emission suppressed ozone formation since the O_3-NO_x-VOC sensitivity was NO_x-limited in CEPO (Supplementary Fig. 3). The coincidence of high emission flux and significant positive trends of marine isoprene could be the reason for decreasing tropospheric O_3 in CEPO (not shown here).

The relative warming in tropical oceans of subsidence (e.g., CEPO) has been linked to decreased lower tropospheric stability and low cloud cover by the proposed mechanism[51] and empirical relationships[52]. Conversely, warmer SST in tropical convection regions is coincident with higher humidity in the upper troposphere, suggesting possible lofting of warm moist air from the surface to the upper troposphere[52]. As the 2015/16 El Niño was the strongest El Niño event ever recorded and CEPO mostly overlaps the Niño-4 region (5 °S to 5 °N, 160 °E to 150 °W), the high isoprene emissions of CEPO during 2015/16 El Niño were potentially linked to organic aerosol formation in the upper troposphere[53]. Furthermore, modeling studies demonstrated that marine isoprene-derived SOA and O_3 could reach as far as hundreds of kilometers inland[11]. Consequently, the change in marine isoprene could potentially affect the regional air quality and global climate.

DISCUSSION

Our study discovered significantly high marine isoprene emissions in CEPO, investigated the main driving parameters of remarkable increasing trends of isoprene fluxes in CEPO, and demonstrated important implications for regional atmospheric photochemistry. Furthermore, coastal oceans and the Tasman Sea exhibited high marine isoprene emissions, while emissions decreased in most open oceans during the study period. Although correlations do not necessarily indicate causation, the positive correlations between marine isoprene emission flux and satellite AOD in most ocean areas suggest that isoprene could be important in SOA formation. NO_2 may play a critical role during aerosol formation from isoprene in the remote ocean air. This study provides an important initial demonstration of the significance of isoprene emission enhancement in the remote tropical ocean. Further measurements of marine isoprene and environmental parameters, particularly over broader tropical oceans, are needed to determine the distributions and impacts of marine organic gas emissions.

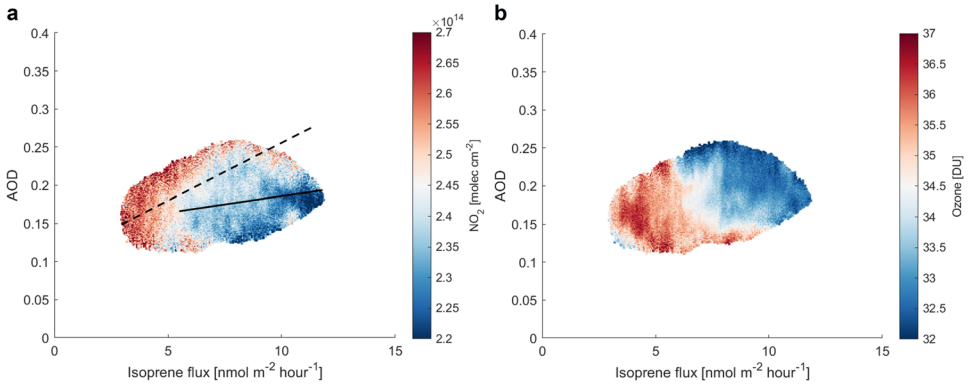

Fig. 5 Comparisons of marine isoprene flux and AOD with monthly tropospheric column densities of NO_2 and ozone in CEPO from August 2015 to December 2020. The data were grouped into 300 × 400 bins with data counts no less than 100 (Supplementary Fig. 7). **a** NO2 is likely to determine the enhancement rate of AOD from marine isoprene in CEPO. The dashed line represents the regression line of binned data with NO_2 column densities higher than 2.5×10^{14} molecules cm^{-2}, and the solid line represents that with NO_2 column densities lower than 2.4×10^{14} molecules cm^{-2}. **b** Lower ozone abundances were observed when marine isoprene emission and AOD were both higher.

METHODS

Isoprene production model

The isoprene production rate p for the predominant phytoplankton species at depth h was established by incorporating a temperature-dependence factor $\alpha_1/(T^2 + \alpha_2 \cdot T + \alpha_3)$ into the log-squared relationship invoked by Gantt et al.[22]:

$$p = EF \cdot \frac{\alpha_1}{(T+\delta)^2 + \alpha_2 \cdot (T+\delta) + \alpha_3} \cdot \ln(I)^2 \quad (1)$$

where EF (in μmol g $Chla^{-1}$ h^{-1}) is a constant emission factor for each PFT (Supplementary Table 1), I and T are the ambient solar radiation (in μE m^{-2} s^{-1}) and temperature (in °C) at the depth h, respectively. The coefficients α_1, α_2, and α_3 were derived as 3.6402, −46.75, and 618.2, respectively, by fitting the rational model to the isoprene production rates of two diatoms species (Supplementary Fig. 6) from the light- and temperature-dependent experiments conducted by Meskhidze et al.[21]. δ is the difference between 23.375 °C and the optimum temperature calculated from the latitudinal gradient in the optimum temperature discovered by Thomas et al.[42]. The details on how to derive the coefficients α_1, α_2, α_3 can be found in Supplementary Note 1.4.

The seawater temperature T at water column depth can be estimated from the satellite-based sea surface observations (i.e., SST, SSH, and WS) by performing the multiple linear regression (MLR) analysis. ISAS temperature gridded fields and climatology, based on the Argo network of profiling floats, were used to train and evaluate the MLR model. The SSH and WS were interpolated to the same grids with the PAR product of Himawari-8 by using the linear interpolation method. More details on training and evaluation of the MLR model can be found in Supplementary Note 1.1.

The reliability of fitted PAR depth profile derived from Beer-Lambert's Law has been verified by the directly measured downwelling PAR profiles[14]. Hence, the light radiation I at depth h of the water column can be estimated from the solar radiation at the sea surface I_0 as follows:

$$I = I_0 \cdot e^{-k_d \cdot h} \quad (2)$$

The satellite PFT identification was performed on the MODIS-Aqua data using the PHYSTWO algorithm (Supplementary Fig. 1b), which is applicable to coastal and open oceans[54]. The six retrieved PFTs are Coccolithophorids bloom, Phaeocystis-like, Diatoms, Synechococcus, Prochlorococcus, and Nanoeukaryotes (see Supplementary Fig. 1b for an example). Their corresponding emission factors and references are listed in Supplementary Table 1.

Cruise measurements demonstrated that isoprene production mainly occurs in seawater deeper than 5 m[55,56]. To better represent the Chl-a concentrations in the whole euphotic layer, our study uses the mean Chl-a concentrations within the euphotic layer instead of the satellite-retrieved sea surface concentrations. The mean Chl-a concentration $\overline{[Chla]}$ can be computed as follows:

$$\overline{[Chla]} = \frac{Chla_{tot}}{H_{max}} \quad (3)$$

where H_{max} is the euphotic layer depth, $Chla_{tot}$ is the column-integrated Chl-a content in mg m^{-2}. $Chla_{tot}$ can be derived from the remotely sensed Chl-a concentration [Chla] by using the statistical relationship given by Morel and Berthon[57]:

$$Chla_{tot} = 38.0 \times [Chla]^{0.425} \quad if\ [Chla] \le 0.5 \quad (4)$$

$$Chla_{tot} = 40.2 \times [Chla]^{0.507} \quad if\ [Chla] > 0.5 \quad (5)$$

where [Chla] is the remotely sensed Chlorophyll concentration in mg m^{-3}.

The euphotic zone depth H_{max}, within which isoprene production can occur in our model, was assumed to extend from the surface to the depth at which the light levels are reduced to 2.5 W m^{-2}, which is the level at which the photosynthesis ceases. This value is the lowest light level for Prochlorococcus[19], here we assume it is applicable for all the PFTs. The depth which represents the maximum possible extent of the planktonic euphotic zone can be determined by using the following equation:

$$H_{max} = -\ln\left(\frac{2.5}{I_0}\right) \cdot k_d^{-1} \quad (6)$$

where k_d is the diffuse attenuation coefficient for PAR. To compute k_d, here we use the revised empirical model provided in ref. [14], Morel and Maritorena[58],

$$k_d = \frac{4.6}{426.3} \times Chla_{tot}^{0.547} \quad if\ Chla_{tot} \le 13.6222\ \text{mg m}^{-2} \quad (7)$$

$$k_d = \frac{4.6}{912.5} \times Chla_{tot}^{0.839} \quad if\ Chla_{tot} > 13.6222\ \text{mg m}^{-2} \quad (8)$$

Isoprene concentration and flux

The isoprene concentration variation rate P caused by phytoplankton production can be established by integrating the

isoprene production rate within the depth H[22]:

$$P = \frac{\beta}{D_{ML}} \cdot \overline{[Chla]} \cdot \int_0^H p\, dh \quad (9)$$

where β is the prefactor set to 86.8798, which was derived by constraining the mean of modeled isoprene seawater concentration to equal that of the in-situ measurements of T/S Osyoro-maru Cruise No. 56 (sampling locations are shown in Supplementary Fig. 1a, comparison between estimates and measurements can be found in Supplementary Fig. 5). D_{ML} is the depth of surface mixed layer in which the isoprene is considered well mixed, and hence the concentration can be treated as uniform, H is the less of H_{max} and D_{ML}. The D_{ML} was calculated by applying the temperature threshold method on the temperature-depth profile, using temperature threshold $\Delta T = 0.2$ °C as the criteria[59].

Due to no significant isoprene accumulation in the depth profile during weeks time frame[60] and the total turnover times of isoprene in the upper ocean varied from 1.4 days (productive waters) to 16 days (oligotrophic waters) in seawater incubation experiments[40], the monthly mean seawater isoprene concentration C_m can be derived by using the steady-state model[27]:

$$P - (k_{bio} + k_{chem}) \cdot C_m - \frac{F_{ocean}}{D_{ML}} - L_{mix} = 0 \quad (10)$$

where k_{bio} and k_{chem} is the biological loss rate and chemical rate constant for all possible loss pathways, their values ($k_{bio} = \mu \overline{[Chla]}^{1.28}$, μ is equal to 0.14, k_{chem} is 0.05 day^{-1}) are given according to the incubation experiments in ref. [40]. F_{ocean} is the seawater isoprene flux. L_{mix} is the loss due to the diffusion downward to the deep ocean, calculated from the following equation:

$$L_{mix} = k_{mix} \cdot C_m \quad (11)$$

where k_{mix} is the vertical mixing rate at the bottom of the mixed layer. The value of k_{mix} is set to -0.005 day^{-1}, which is suggested by a modeling study[61] and is the median value of the cruise measurements[40].

The marine isoprene flux at the ocean–atmosphere interface is described as the sum of the seawater isoprene flux and the SML flux. Seawater isoprene flux is due to the phytoplankton production and biochemical loss in the water column, whereas the SML flux results from the photosensitized reactions in the SML. The detailed calculation processes for calculating seawater isoprene flux and the SML flux are provided in Supplementary Note 1.2 and Supplementary Note 1.3.

Trend analysis

We evaluated trends of the time series in marine isoprene flux, the environmental drivers (Chl-a concentration, SST, PAR, wind speed), AOD, ozone, formaldehyde, and NO_2 at each grid cell. Trend analysis was performed on the time series using the Mann–Kendall (MK) test[37], a robust non-parametric test for trend detection. The slope of linear trends was determined using the Theil–Sen estimator[38,39]. Here, we set the significance level at 0.05, which means the trend is significant when Z statistic is larger than 1.96 or less than −1.96. The uncertainties on the estimate of the non-zero trend slope were quantified using the Exclude-one and Estimate Slope (EES) method[62], with a significance level of 5%. The statistical analysis of absolute and relative trends in selected ocean regions was only performed upon significant trends. The confidence levels for the isoprene emission fluxes are shown in Supplementary Fig. 11.

Sensitivity test

A set of sensitivity analyses were designed to assess the model response to six driving parameters, namely Chl-a, SST, PAR, EF, H_{max}, and D_{ML}. One base case was performed in which all six parameters were held spatially and temporally constant to the median values in the study domain, and other six simulations were made in which all but one of these parameters were held constant. The differences between each of these six simulations and the base case for March 2020 are shown in Supplementary Figs. 12 and 13 as an example to quantify the contribution of each parameter to the spatial distributions of the marine isoprene emissions and seawater isoprene concentrations, respectively. The Chl-a, SST, and PAR have the greatest impact on the estimates of marine isoprene emissions in most of the study domains (Supplementary Fig. 12a–c). In Supplementary Fig. 12d, the contribution of EF to the estimates of isoprene emissions ranges from −55% to 37%, highlighting the importance of a good measurement of EF for specific PFT. As H_{max} and D_{ML} are related to the assumptions of our model, the low percentage differences (lower than 10%) of H_{max} and D_{ML} in most of the study domains suggest the robustness of our results to the assumptions (Supplementary Fig. 12e, f). Therefore, our work indicates Chl-a, SST, PAR, and EF have higher requirements in their accuracy due to their significant contributions to marine isoprene emissions.

DATA AVAILABILITY

Research products of Chla, SST, PAR, and AOD (produced from Himawari-8) used in this paper were supplied by the P-Tree System (https://www.eorc.jaxa.jp/ptree/faq.html), Japan Aerospace Exploration Agency (JAXA). GlobColour data (http://globcolour.info) used in this study has been developed, validated, and distributed by ACRI-ST, France. The SSH data was downloaded from https://resources.marine.copernicus.eu/?option=com_csw&view=details&product_id=GLOBAL_REANALYSIS_PHY_001_030. The monthly averaged reanalysis of wind speed and wind stress (https://doi.org/10.24381/cds.f17050d7) were downloaded from the Copernicus Climate Change Service (C3S) Climate Data Store. The ISAS-13-CLIM temperature gridded climatology can be found at https://doi.org/10.17882/45946. The ISAS gridded fields of temperature is available at https://doi.org/10.17882/52367. The isoprene seawater concentration data during T/S Osyoro-maru Cruise No. 56 is available at https://ads.nipr.ac.jp/dataset/A20191216-005. The tropospheric column NO_2 product is available at https://disc.gsfc.nasa.gov/datasets/OMNO2d_003/summary. The tropospheric column Formaldehyde product is available at https://disc.gsfc.nasa.gov/datasets/OMHCHOd_003/summary. The tropospheric column O_3 product is available at https://acd-ext.gsfc.nasa.gov/Data_services/cloud_slice/new_data.html.

CODE AVAILABILITY

Codes used to generate the results of this study are available from the authors on reasonable request.

Received: 20 May 2022; Accepted: 12 October 2022;
Published online: 02 November 2022

REFERENCES

1. Meskhidze, N. & Nenes, A. Phytoplankton and cloudiness in the southern ocean. *Science* **314**, 1419–1423 (2006).
2. Claeys, M. et al. Formation of secondary organic aerosols through photooxidation of isoprene. *Science* **303**, 1173–1176 (2004).
3. Henze, D. K. & Seinfeld, J. H. Global secondary organic aerosol from isoprene oxidation. *Geophys. Res. Lett.* **33**, L09812 (2006).
4. Ziemann, P. J. Thwarting the seeds of clouds. *Nature* **461**, 353–354 (2009).
5. Kiendler-Scharr, A. et al. New particle formation in forests inhibited by isoprene emissions. *Nature* **461**, 381–384 (2009).
6. Guenther, A. et al. Estimates of global terrestrial isoprene emissions using MEGAN (model of emissions of gases and aerosols from nature). *Atmos. Chem. Phys.* **6**, 3181–3210 (2006).
7. Gu, D. et al. Airborne observations reveal elevational gradient in tropical forest isoprene emissions. *Nat. Commun.* **8**, 15541 (2017).
8. Yu, Z. & Li, Y. Marine volatile organic compounds and their impacts on marine aerosol—a review. *Sci. Total Environ.* **768**, 145054 (2021).
9. Broadgate, W. J., Liss, P. S. & Penkett, S. A. Seasonal emissions of isoprene and other reactive hydrocarbon gases from the ocean. *Geophys. Res. Lett.* **24**, 2675–2678 (1997).

10. Hu, Q. et al. Secondary organic aerosols over oceans via oxidation of isoprene and monoterpenes from Arctic to Antarctic. *Sci. Rep.* **3**, 2280 (2013).
11. Gantt, B., Meskhidze, N., Zhang, Y. & Xu, J. The effect of marine isoprene emissions on secondary organic aerosol and ozone formation in the coastal United States. *Atmos. Environ.* **44**, 115–121 (2010).
12. Gantt, B., Meskhidze, N. & Carlton, A. G. The contribution of marine organics to the air quality of the western United States. *Atmos. Chem. Phys.* **10**, 7415–7423 (2010).
13. Bonsang, B., Polle, C. & Lambert, G. Evidence for marine production of isoprene. *Geophys. Res. Lett.* **19**, 1129–1132 (1992).
14. Booge, D. et al. Marine isoprene production and consumption in the mixed layer of the surface ocean—a field study over two oceanic regions. *Biogeosciences* **15**, 649–667 (2018).
15. Carpenter, L. J., Archer, S. D. & Beale, R. Ocean-atmosphere trace gas exchange. *Chem. Soc. Rev.* **41**, 6473–6506 (2012).
16. Ooki, A., Nomura, D., Nishino, S., Kikuchi, T. & Yokouchi, Y. A global-scale map of isoprene and volatile organic iodine in surface seawater of the A Northwest Pacific, Indian, and Southern Oceans. *J. Geophys. Res. Oceans* **120**, 4108–4128 (2015).
17. Colomb, A., Yassaa, N., Williams, J., Peeken, I. & Lochte, K. Screening volatile organic compounds (VOCs) emissions from five marine phytoplankton species by head space gas chromatography/mass spectrometry (HS-GC/MS). *J. Environ. Monit.* **10**, 325 (2008).
18. Exton, D. A., Suggett, D. J., McGenity, T. J. & Steinke, M. Chlorophyll-normalized isoprene production in laboratory cultures of marine microalgae and implications for global models. *Limnol. Oceanogr.* **58**, 1301–1311 (2013).
19. Shaw, S. L., Chisholm, S. W. & Prinn, R. G. Isoprene production by Prochlorococcus, a marine cyanobacterium, and other phytoplankton. *Mar. Chem.* **80**, 227–245 (2003).
20. Broadgate, W. J., Malin, G., Küpper, F. C., Thompson, A. & Liss, P. Isoprene and other non-methane hydrocarbons from seaweeds: a source of reactive hydrocarbons to the atmosphere. *Mar. Chem.* **88**, 61–73 (2004).
21. Meskhidze, N., Sabolis, A., Reed, R. & Kamykowski, D. Quantifying environmental stress-induced emissions of algal isoprene and monoterpenes using laboratory measurements. *Biogeosciences* **12**, 637–651 (2015).
22. Gantt, B., Meskhidze, N. & Kamykowski, D. A new physically-based quantification of marine isoprene and primary organic aerosol emissions. *Atmos. Chem. Phys.* **9**, 4915–4927 (2009).
23. Sinha, V. et al. Air-sea fluxes of methanol, acetone, acetaldehyde, isoprene and DMS from a Norwegian fjord following a phytoplankton bloom in a mesocosm experiment. *Atmos. Chem. Phys.* **7**, 739–755 (2007).
24. Exton, D. A., Suggett, D. J., Steinke, M. & McGenity, T. J. Spatial and temporal variability of biogenic isoprene emissions from a temperate estuary: Estuarine isoprene emissions. *Glob. Biogeochem. Cycle* **26**, GB2012 (2012).
25. Rodríguez-Ros, P. et al. Distribution and drivers of marine isoprene concentration across the southern ocean. *Atmosphere* **11**, 556 (2020).
26. Luo, G. & Yu, F. A numerical evaluation of global oceanic emissions of α-pinene and isoprene. *Atmos. Chem. Phys.* **10**, 2007–2015 (2010).
27. Palmer, P. I. & Shaw, S. L. Quantifying global marine isoprene fluxes using MODIS chlorophyll observations. *Geophys. Res. Lett.* **32**, L09805 (2005).
28. Booge, D. et al. Can simple models predict large-scale surface ocean isoprene concentrations? *Atmos. Chem. Phys.* **16**, 11807–11821 (2016).
29. Arnold, S. R. et al. Relationships between atmospheric organic compounds and air-mass exposure to marine biology. *Environ. Chem.* **7**, 232 (2010).
30. Arnold, S. R. et al. Evaluation of the global oceanic isoprene source and its impacts on marine organic carbon aerosol. *Atmos. Chem. Phys.* **9**, 1253–1262 (2009).
31. Donaldson, D. J. & Vaida, V. The influence of organic films at the air-aqueous boundary on atmospheric processes. *Chem. Rev.* **106**, 1445–1461 (2006).
32. Novak, G. A. & Bertram, T. H. Reactive VOC production from photochemical and heterogeneous reactions occurring at the air-ocean interface. *Accounts Chem. Res.* **53**, 1014–1023 (2020).
33. Ciuraru, R. et al. Unravelling new processes at interfaces: photochemical isoprene production at the sea surface. *Environ. Sci. Technol.* **49**, 13199–13205 (2015).
34. Brüggemann, M., Hayeck, N. & George, C. Interfacial photochemistry at the ocean surface is a global source of organic vapors and aerosols. *Nat. Commun.* **9**, 2101 (2018).
35. Kim, M. J. et al. Air-sea exchange of biogenic volatile organic compounds and the impact on aerosol particle size distributions: air-sea exchange of biogenic VOCs. *Geophys. Res. Lett.* **44**, 3887–3896 (2017).
36. de Boyer Montégut, C., Madec, G., S. Fischer, A., Lazar, A. & Iudicone, D. Mixed layer depth over the global ocean: An examination of profile data and a profile-based climatology. *J. Geophys. Res.* **109**, C12003 (2004).
37. Kendall, M. G. & Gibbons, J. D. *Rank Correlation Methods* (Oxford University Press, 1990).
38. Theil, H. A rank-invariant method of linear and polynomial regression analysis. I. *Proc. K. Ned. Akad. Wet.* **53**, 386–392 (1950).
39. Sen, P. Estimates of the regression coefficient based on Kendall's tau. *J. Am. Stat. Assoc.* **63**, 1379–1389 (1968).
40. Simó, R., Cortés-Greus, P., Rodríguez-Ros, P. & Masdeu-Navarro, M. Substantial loss of isoprene in the surface ocean due to chemical and biological consumption. *Commun. Earth Environ.* **3**, 20 (2022).
41. Anderson, S. I., Barton, A. D., Clayton, S., Dutkiewicz, S. & Rynearson, T. A. Marine phytoplankton functional types exhibit diverse responses to thermal change. *Nat. Commun.* **12**, 6413 (2021).
42. Thomas, M. K., Kremer, C. T., Klausmeier, C. A. & Litchman, E. A global pattern of thermal adaptation in marine phytoplankton. *Science* **338**, 1085–1088 (2012).
43. Righetti, D., Vogt, M., Gruber, N., Psomas, A. & Zimmermann, N. E. Global pattern of phytoplankton diversity driven by temperature and environmental variability. *Sci. Adv.* **5**, eaau6253 (2019).
44. Rap, A. et al. Natural aerosol direct and indirect radiative effects. *Geophys. Res. Lett.* **40**, 3297–3301 (2013).
45. Quinn, P. K., Coffman, D. J., Johnson, J. E., Upchurch, L. M. & Bates, T. S. Small fraction of marine cloud condensation nuclei made up of sea spray aerosol. *Nat. Geosci.* **10**, 674–679 (2017).
46. Mayer, K. J. et al. Secondary marine aerosol plays a dominant role over primary sea spray aerosol in cloud formation. *ACS Central Sci.* **6**, 2259–2266 (2020).
47. Bates, K. H. & Jacob, D. J. A new model mechanism for atmospheric oxidation of isoprene: global effects on oxidants, nitrogen oxides, organic products, and secondary organic aerosol. *Atmos. Chem. Phys.* **19**, 9613–9640 (2019).
48. Zavarsky, A. et al. The influence of air-sea fluxes on atmospheric aerosols during the summer monsoon over the tropical Indian Ocean: air-sea fluxes in the Indian Ocean. *Geophys. Res. Lett.* **45**, 418–426 (2018).
49. Ziemke, J. R. et al. Tropospheric ozone determined from Aura OMI and MLS: evaluation of measurements and comparison with the Global Modeling Initiative's Chemical Transport Model. *J. Geophys. Res.* **111**, D19303 (2006).
50. Surratt, J. D. et al. Reactive intermediates revealed in secondary organic aerosol formation from isoprene. *Proc. Natl. Acad. Sci. USA* **107**, 6640–6645 (2010).
51. Andrews, T. & Webb, M. J. The dependence of global cloud and lapse rate feedbacks on the spatial structure of tropical Pacific warming. *J. Clim.* **31**, 641–654 (2018).
52. Mackie, A., Brindley, H. E. & Palmer, P. I. Contrasting observed atmospheric responses to tropical sea surface temperature warming patterns. *J. Geophys. Res.-Atmos.* **126**, e2020JD033564 (2021).
53. Palmer, P. I., Marvin, M. R., Siddans, R., Kerridge, B. J. & Moore, D. P. Nocturnal survival of isoprene linked to formation of upper tropospheric organic aerosol. *Science* **375**, 562–566 (2022).
54. Correa-Ramirez, M., Morales, C., Letelier, R., Anabalón, V. & Hormazabal, S. Improving the remote sensing retrieval of phytoplankton functional types (PFT) using empirical orthogonal functions: a case study in a coastal upwelling region. *Remote Sens.* **10**, 498 (2018).
55. Tran, S. et al. A survey of carbon monoxide and non-methane hydrocarbons in the Arctic Ocean during summer 2010. *Biogeosciences* **10**, 1909–1935 (2013).
56. Hackenberg, S. C. et al. Potential controls of isoprene in the surface ocean: Isoprene controls in the surface ocean. *Glob. Biogeochem. Cycle* **31**, 644–662 (2017).
57. Morel, A. & Berthon, J. Surface pigments, algal biomass profiles, and potential production of the euphotic layer: relationships reinvestigated in view of remote-sensing applications: production computed from space-acquired data. *Limnol. Oceanogr.* **34**, 1545–1562 (1989).
58. Morel, A. & Maritorena, S. Bio-optical properties of oceanic waters: a reappraisal. *J. Geophys. Res.-Oceans* **106**, 7163–7180 (2001).
59. Jeong, Y., Hwang, J., Park, J., Jang, C. J. & Jo, Y. Reconstructed 3-D ocean temperature derived from remotely sensed sea surface measurements for mixed layer depth analysis. *Remote Sens.* **11**, 3018 (2019).
60. Moore, R. M. & Wang, L. The influence of iron fertilization on the fluxes of methyl halides and isoprene from ocean to atmosphere in the SERIES experiment. *Deep-Sea Res. Part II-Top. Stud. Oceanogr.* **53**, 2398–2409 (2006).
61. Conte, L., Szopa, S., Aumont, O., Gros, V. & Bopp, L. Sources and sinks of isoprene in the global open ocean: simulated patterns and emissions to the atmosphere. *J. Geophys. Res. Oceans* **125**, e2019JC015946 (2020).
62. Onyutha, C. Statistical analyses of potential evapotranspiration changes over the period 1930-2012 in the Nile River riparian countries. *Agric. For. Meteorol.* **226-227**, 80–95 (2016).

ACKNOWLEDGEMENTS

The authors would like to thank the two anonymous reviewers for their constructive comments. This work was supported by the Hong Kong Research Grants Council (26304921), Hong Kong Environmental Conservation Fund (78/2019), and Department of Science and Technology of Guangdong Province in China (2019B121205004).

AUTHOR CONTRIBUTIONS

W.Z. and D.G. designed the project, proposed the methodology, analyzed the results, and wrote the manuscript. W.Z. developed the model schemes, analyzed satellite observation data, and conducted model simulations.

COMPETING INTERESTS

The authors declare no competing interests.

ADDITIONAL INFORMATION

Supplementary information The online version contains supplementary material available at https://doi.org/10.1038/s41612-022-00311-0.

Correspondence and requests for materials should be addressed to Dasa Gu.

Reprints and permission information is available at http://www.nature.com/reprints

Publisher's note Springer Nature remains neutral with regard to jurisdictional claims in published maps and institutional affiliations.